JGR Space Physics

RESEARCH ARTICLE
10.1029/2019JA027443

Variations of Mesospheric Neutral Winds and Tides Observed by a Meteor Radar Chain Over China During the 2013 Sudden Stratospheric Warming

Na Li[1,2,3,4], Xiaoli Luan[1,3,4], Jiuhou Lei[1,3,4], O. S. Bolaji[5,6], Charles Owolabi[1,7], Jinsong Chen[2], Zhengwen Xu[2], Guozhu Li[8], and Baiqi Ning[8]

[1]CAS Key Laboratory of Geospace Environment, School of Earth and Space Sciences, University of Science and Technology of China, Hefei, China, [2]National Key Laboratory of Electromagnetic Environment, China Research Institute of Radio Wave Propagation, Qingdao, China, [3]CAS Center for Excellence in Comparative Planetology, University of Science and Technology of China, Hefei, China, [4]Mengcheng National Geophysical Observatory, University of Science and Technology of China, Hefei, China, [5]Department of Physics, University of Lagos, Lagos, Nigeria, [6]Department of Physics, University of Tasmania, Hobart, Tasmania, Australia, [7]Department of Physics, Federal University of Technology Akure, Akure, Nigeria, [8]Key Laboratory of Earth and Planetary Physics, Institute of Geology and Geophysics, Chinese Academy of Sciences, Beijing, China

Key Points:
- Neutral wind observations from a meteor radar chain over China are utilized to study the MLT responses to the SSW in 2013
- Latitudinal structures of tides and winds are investigated during the SSW
- The diurnal and semidiurnal tides of neutral winds show a large decrease followed by an increase during the SSW

Correspondence to:
J. Lei,
leijh@ustc.edu.cn

Citation:
Li, N., Luan, X., Lei, J., Bolaji, O. S., Owolabi, C., Chen, J., et al. (2020). Variations of mesospheric neutral winds and tides observed by a meteor radar chain over China during the 2013 sudden stratospheric warming. *Journal of Geophysical Research: Space Physics*, *125*, e2019JA027443. https://doi.org/10.1029/2019JA027443

Received 21 SEP 2019
Accepted 24 MAR 2020
Accepted article online 6 APR 2020

Abstract The neutral winds in the mesospheric and lower thermospheric region obtained from a meteor radar chain within the latitudinal range of 18–53°N were decomposed to examine the latitudinal structures of the tides and mean winds during the sudden stratospheric warming (SSW) event in 2013. The zonal wind reversed from eastward to westward and the westward wind was larger at middle latitudes than that at low latitudes during the SSW. Meanwhile, a sharp increase in the northward wind was noticeable at all stations. The amplitudes of the diurnal and semidiurnal tides decreased from 5 to 13 January and increased subsequently. At the same time, the terdiurnal tides increased in amplitude, especially at Beijing, Wuhan, and Kunming, in response to the SSW. Moreover, the tidal phases showed a large shift that corresponded to a great increase in tidal wavelengths in the semidiurnal and terdiurnal components. The wavelet analysis further revealed that the quasi 6-day wave oscillations dominated in the winds at Kunming and Sanya stations, as well as the quasi 16-day wave dominated in the zonal wind, and the quasi 11-day and 16-day waves were prevailing in the meridional winds at Beijing and Wuhan. In the same vein, the quasi 16-day and quasi 11-day waves were prominent in the zonal and meridional winds during 1–18 January at Mohe. Therefore, the tide-planetary wave interactions played a significant role in modulating the behaviors of the mesospheric and lower thermospheric dynamics during the SSW event.

1. Introduction

In the winter polar region, the horizontal gradient of the thermal condition caused by the land-sea distribution generates the large-scale planetary waves (PWs) continuously (Reed, 1963). PWs propagate upward and northward, with their amplitudes increasing exponentially with altitude. The nonlinear interaction of PWs and mean zonal circulation induces the wave packet broken and releases the momentum into background atmosphere (Beard et al., 1999; Coy et al., 2011; Martineau & Son, 2015; Matthias et al., 2012; Siskind et al., 2010). As a result, the polar stratospheric temperature warms profoundly by tens of degrees and the middle atmospheric temperature cools down within a short time period, which is characterized as a sudden stratospheric warming (SSW) event. The SSW is an extreme terrestrial weather that usually occurs in the winter polar stratosphere of the Northern Hemisphere and subsequently affects global-scale coupling dynamics process (Pancheva et al., 2008; Shepherd et al., 2007). According to World Meteorological Organization, a stratospheric warming can be classified as a major warming, when the zonal mean wind in the stratosphere layer at 60°N and 10 hPa changes its direction from eastward to westward, or a minor one, when the zonal mean wind in the stratosphere layer does not reverse its direction and its speed becomes weaken (Labitzke & Naujokar, 2000).

The zonal and meridional winds in the mesospheric and lower thermospheric (MLT) region during wintertime are generally eastward and northward over the middle and low latitudes, respectively. However, the SSW can significantly affect the variations of dynamical structures in the MLT region

(Chandran et al., 2013; Hoffmann et al., 2007; Ma et al., 2017; Wit et al., 2015) and even in the ionosphere (Bolaji et al., 2016; Owolabi et al., 2019; Siddiqui et al., 2015; Yamazaki et al., 2012). The neutral winds after the onset of SSW are observed to reverse to westward and southward (Chen et al., 2012; Dowdy et al., 2007; Lima et al., 2012; Sathishkumar & Sridharan, 2009; Wang & Alexander, 2009; Yuan et al., 2012). This reversal of meridional winds during SSW event could be related to significant increase in the gravity waves activities (Chandran et al., 2014; Yamashita et al., 2010). The westward reversal of zonal winds during the SSW is ascribed to the interaction between the background wind and the upward propagating PW that reaches the line of zero wind (critical layer) in the upper mesosphere (Matsuno, 1971). Meanwhile, the nonlinear interaction between PW and atmospheric mean flow causes the growth of the semidiurnal tidal component (Bhattacharya et al., 2004; Sathishkumar & Sridharan, 2013). Chen et al. (2012), Sridharan (2017), He et al. (2017), and Koushik et al. (2018) reported the enhancements in the migrating tidal components (diurnal, semidiurnal, and terdiurnal tides) and their associated quasi 2- and 16-day waves during the SSW events. In addition, the in situ satellite observations and numerical models have also applied to study the variations of neutral winds and their tides in the MLT region during the SSW events (Lin et al., 2012; Matsuno, 1971; Niciejewski et al., 2006; Pedatella & Forbes, 2010; Pedatella & Liu, 2013; Sassi et al., 2013; Sridharan, 2017). However, most of these studies were based on the observations derived from one or two stations. The latitudinal dependences of the effects of the SSW on the MLT neutral winds are rarely explored from the observational view.

In this work, we focus on the SSW event that occurred during January 2013 when the neutral wind observations from a meteor radar chain along the longitude 120°E within the latitudinal range of 18–53°N were available. These winds observations at multiple stations provided a unique opportunity to examine the latitudinal variations of neutral winds, tides, and PWs in response to the SSW.

2. Meteor Radar Data and Method of Analysis

Meteor radars can provide nearly continuous information on winds and meteors in the upper mesosphere and lower thermosphere region (70–110 km) with the temporal and vertical resolutions of about 1 hr and 2 km, respectively. With the support of Chinese Meridian Project, four meteor radars were installed at Mohe (53.5°N, 122.3°E), Beijing (40.3°N, 116.2°E), Wuhan (30.5°N, 114.6°E), and Sanya (18.3°N, 109.6°E) in 2011 around the geographic longitude of 120°E. Further details regarding these meteor radars can be found in previous literatures (Liu et al., 2017; Ma et al., 2017; Xiong et al., 2013; Yu et al., 2013, 2015). Besides these four radars, the Kunming meteor radar (25.6°N, 103.8°E), which belongs to the China Research Institute of Radio Wave Propagation, has been operated since year 2011. All of these five meteor radars, designed by the ATRAD meteor detection radar series, are essentially identical to the Buckland Park meteor radar system described by Holdsworth et al. (2004). The geographical locations of these radars and their basic information are given in Figure 1 and Table 1.

Continuous zonal (U) and meridional (V) wind observations between 1 December 2012 and 28 February 2013 have been analyzed to obtain the mean wind and tidal waves. There were data gaps from 17 to 19 February at Beijing station and from 6 to 7 December at Sanya. These data gaps are due to interruptions in the data recording. We decomposed U and V into four components, including mean wind, diurnal tide (period = 24 hr), semidiurnal tide (period = 12 hr), and terdiurnal tide (period = 8 hr) using the least squares method. The amplitudes of quarter diurnal (6 hr) tide and other higher-frequency modes are insignificant and are thus ignored in this study.

It is well known that the thermal tides of the upper atmosphere include the nonmigrating and migrating components. It is difficult to isolate these tidal components due to lack of longitudinal information from the meteor radar chain over the limited region. In addition, the magnitudes of the nonmigrating tidal components are usually small compared to those of migrating tides. Hence, the nonmigrating tides are not distinguished in this work. The U and V are then expressed as the combination of different tidal components as shown in equation 1. For the harmonic fitting, a 4-day data window with 1-day shifting was applied at each height to the wind field data. In each harmonic fitting, 24-hr data sets are used to calculate the diurnal, semidiurnal, and terdiurnal tidal amplitudes and phases:

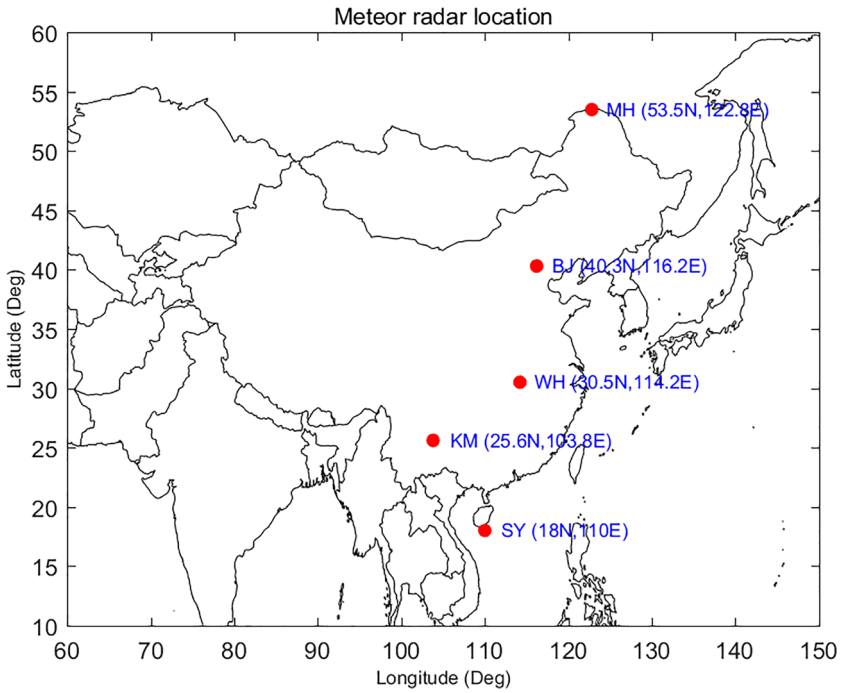

Figure 1. Location of the meteor radar chain including the stations of Mohe, Beijing, Wuhan, Kunming, and Sanya.

$$y_w(\theta, h, t) = y_{w_0} + \sum_{f=1}^{3} A_w^f(\theta, h)\cos\left(\frac{2\pi f}{24}t - \varphi_w^f\right) \quad (1)$$

where θ, h, t, and f are the latitude, altitude, universal time, and frequency, respectively. y_w is the zonal (U) or meridional (V) wind observed by the meteor radar. y_{w_0} is the mean wind, and A_w^f and φ_w^f are the tidal amplitudes and phases, respectively. $f = 1$, 2, and 3 in equation 1 represents tidal period of 24, 12, and 8 hr, respectively. The phase is the time when tidal amplitude reaches its peak value.

3. Results

3.1. Stratospheric Temperature and Zonal Winds in the 2013 SSW Event

The features of the mean zonal stratospheric temperature profile at 90°N (top panel), 60°N (middle panel), and mean zonal wind at 60°N (bottom panel) at the 10-hPa pressure level are displayed in Figure 2. The daily horizontal wind and temperature in these plots are the National Center for Environmental Prediction reanalysis data from National center atmospheric research (NCEP/NCAR) reanalysis data (Kalnay et al., 1996) in the Northern Hemisphere from 1 December 2012 to 28 February 2013. As shown in Figure 2, the stratospheric temperature at 90°N showed a dramatic variation during the entire period of this event. The temperature had several peaks with ~244 K on 7 January, ~240 K on 13 January, and ~236 K on 15 January. The temperature declined gradually from around 23

Table 1
Key Parameters of the Meteor Radars Used in This Work

	Mohe	Beijing	Wuhan	Kunming	Sanya
Freqency (MHz)	38.9	38.9	38.9	37.5	47.5
Time res	1 hr	1 hr	1 hr	1 hr	1 hr
Range_res	2 km	2 km	2 km	2 km	2 km
Peak power	20 kW	20 kW	20 kW	20 kW	20 kW
Pulse width	24 μs	24 μs	24 μs	24 μs	24 μs
Height (km)	70–110	70–110	70–110	70–110	70–110

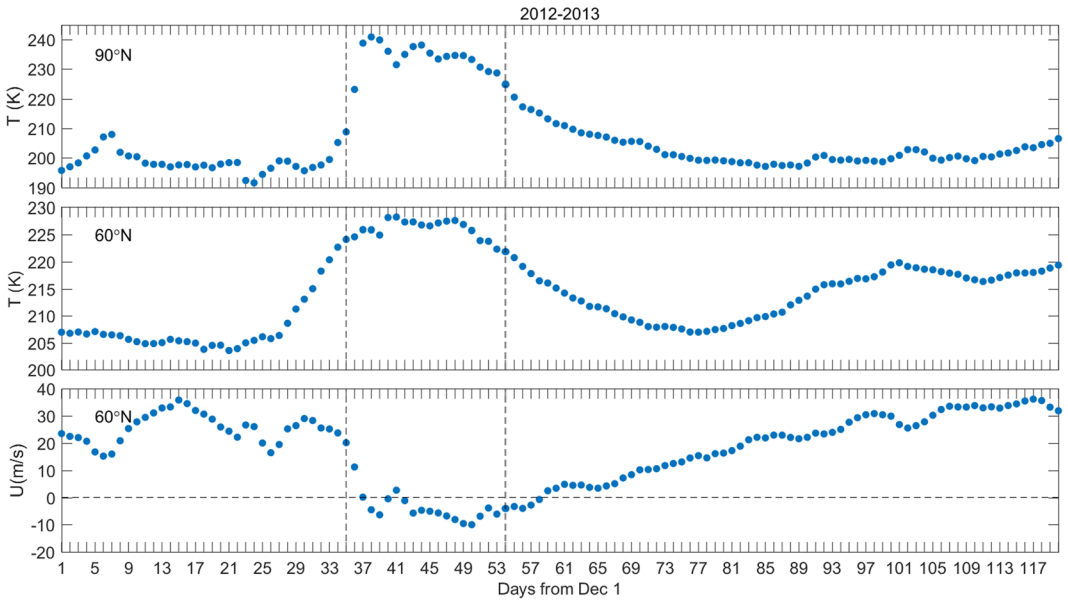

Figure 2. Variations of stratospheric temperature and zonal wind at 30 km for the winter in 2012–2013. (top) Stratospheric temperature at 90°N. (middle) Stratospheric temperature at 60°N. (bottom) Mean zonal wind at 60°N.

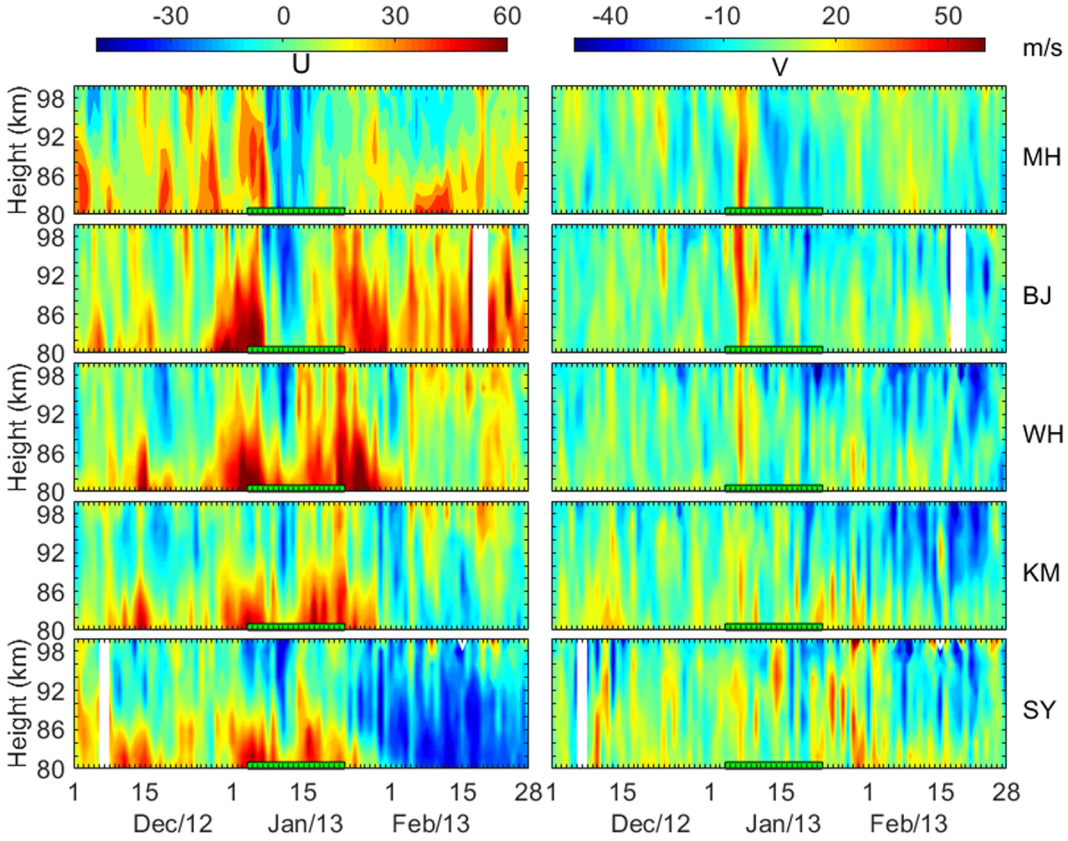

Figure 3. The altitudinal and temporary variation of observed zonal (left) and meridional (right) winds during 1 December 2012 to 28 February 2013 at Mohe (MH), Beijing (BJ), Wuhan (WH), Kunming (KM), and Sanya (SY). The green bar in the *X* axis denotes the period of 2013 SSW.

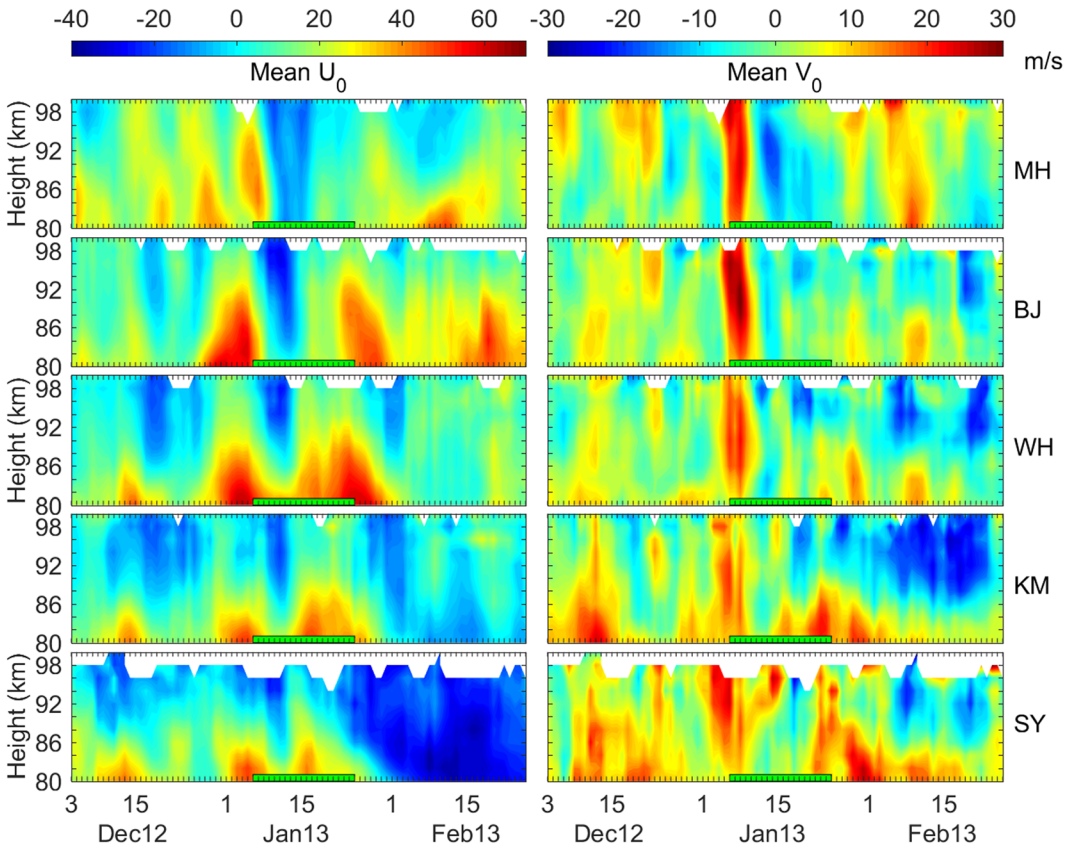

Figure 4. Variations of mean winds as a function of altitude and date during the 2013 SSW at Mohe, Beijing, Wuhan, Kunming, and Sanya.

January and reached its normal magnitude of ~190 K around late February 2013. Meanwhile, the stratospheric temperature at 60°N increased suddenly from ~210 K on 29 December to ~227 K on 7 January and then remained at a high level until 17 January. The westward wind lasted for more than 21 days with a maximum speed of ~ −10 m/s. After 27 January, the stratosphere began to recover to its quiescent condition. According to the World Meteorological Organization criteria (Labitzke & Naujokar, 2000), this is a major SSW event with the onset on 6 January.

3.2. Variations of Mean Winds in the MLT

Figures 3 and 4 show the variations of neutral winds and background winds during the 2013 SSW. The horizontal green line in each panel indicated the SSW period. For the zonal wind component, its features prior to the SSW onset (1 to 3 January) varied significantly from location. One major difference prior to the SSW onset was that the eastward wind was prevailing at all altitudes at Mohe station, while below 94 and 92 km at Beijing and Wuhan stations. Moreover, at lower latitudes (Kunming and Sanya), the eastward wind showed an increase below 88 km. Prior to the SSW onset, the peak of eastward wind was about 61 m/s around 82 km at Beijing, Wuhan, Kunming, and Sanya. However, the zonal wind at Mohe was 44 m/s at 82–92 km.

During the 2013 SSW event (4 January), the eastward wind became weaker and reversed to westward on 7 January at all stations (Figures 3 and 4 on the left column). The covering height range of westward reversal decreased with the decreasing latitude. This westward wind lasted longer at the middle-latitude stations (Mohe, Beijing, and Wuhan) than that at the low-latitude stations (Kunming and Sanya). Hence, the reversal from westward to eastward wind was earlier at the lower latitudes (around 14 January). The westward wind reversal happened around 16 January at Mohe, 13 January at Beijing, 12 January at Wuhan, and 11 January at Kunming and Sanya. After the SSW event, this eastward wind at Mohe, Beijing, and Wuhan remained for a longer period until the end of February. Around 28 and 22 January, the eastward wind

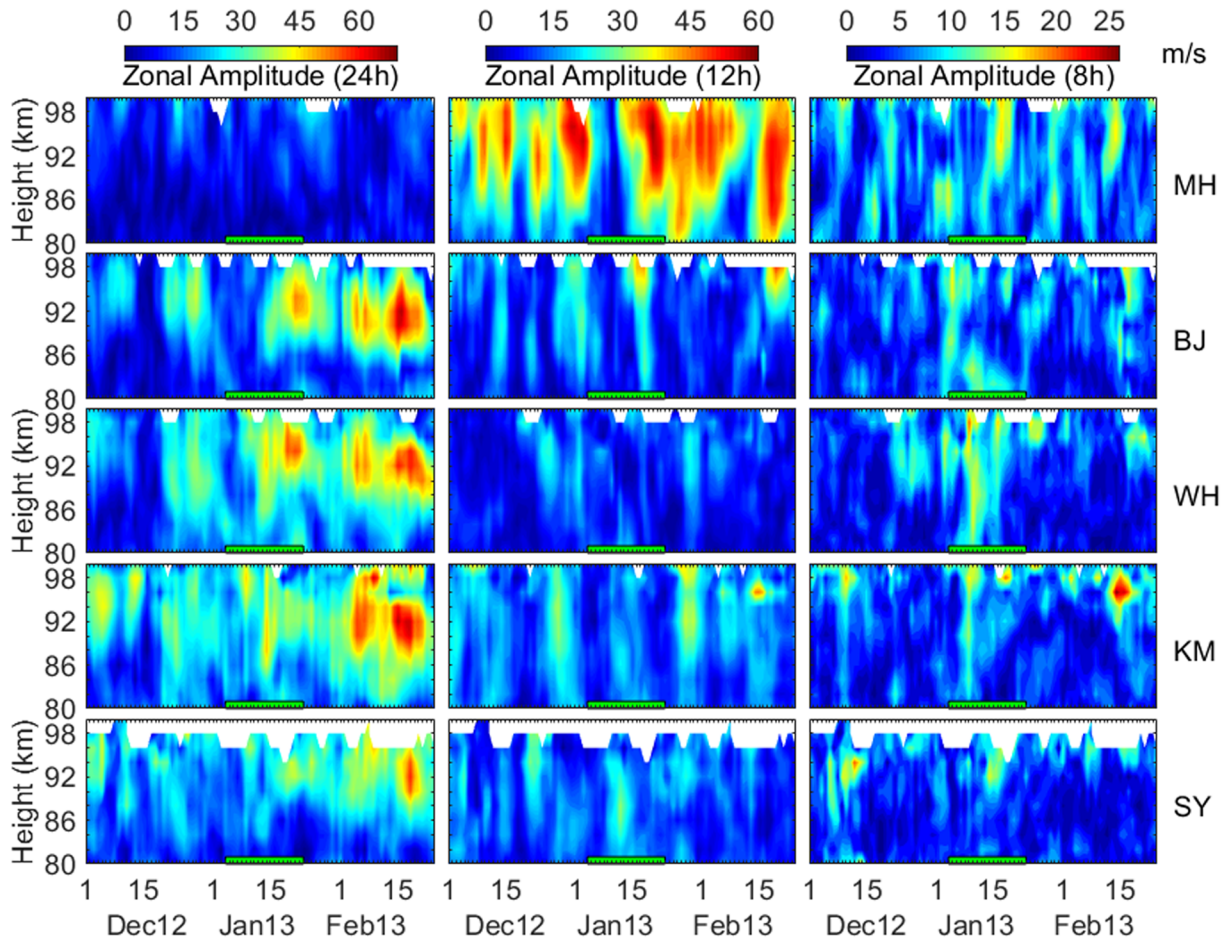

Figure 5. Variations of diurnal (left column), semidiurnal (middle column), and terdiurnal (right column) amplitudes in zonal winds as a function of altitude and date during the 2013 SSW at Mohe, Beijing, Wuhan, Kunming, and Sanya.

reversed to westward again at Kunming and Sanya and the westward wind remained until the end of February.

As shown in Figures 3 and 4, the northward wind at all stations increased prominently at the onset time of the SSW. After that, the northward wind became weaker at the low latitudes and reserved to southward at the middle latitudes around 10 January. Overall, the magnitude and the period of prevailing wind showed clearly latitudinal-dependent structure. In other words, the SSW revealed significant and different effects on the MLT dynamics at the middle and low latitudes.

3.3. Variations of Neutral Wind Tides

Figures 5 and 6 display the tidal amplitudes of the zonal and meridional winds that based on this radar chain. It is clear that tidal amplitudes showed prominent variations with latitudes during the 2013 SSW. The diurnal amplitude of the zonal wind was higher at Beijing, Wuhan, and Kunming, moderate at Sanya and lower at Mohe. The diurnal amplitude of the meridional wind increased as the latitude decreased. For instance, the amplitude was ~28 m/s at Mohe and ~113 m/s at Sanya. As shown in Figures 5 and 6, the diurnal amplitudes of zonal and meridional winds increased from around 21 December to 4 January at all stations, and the increased amplitude remained for a longer period at higher latitudes. The diurnal amplitudes were small before the SSW, while greater magnitudes were seen after the SSW. In addition, the diurnal amplitude of the meridional wind was larger than that of the zonal wind.

Furthermore, the semidiurnal amplitude of the zonal wind showed clear variations during the entire disturbed periods at Mohe (Figure 5, middle column) as compared with those at other stations. Before the

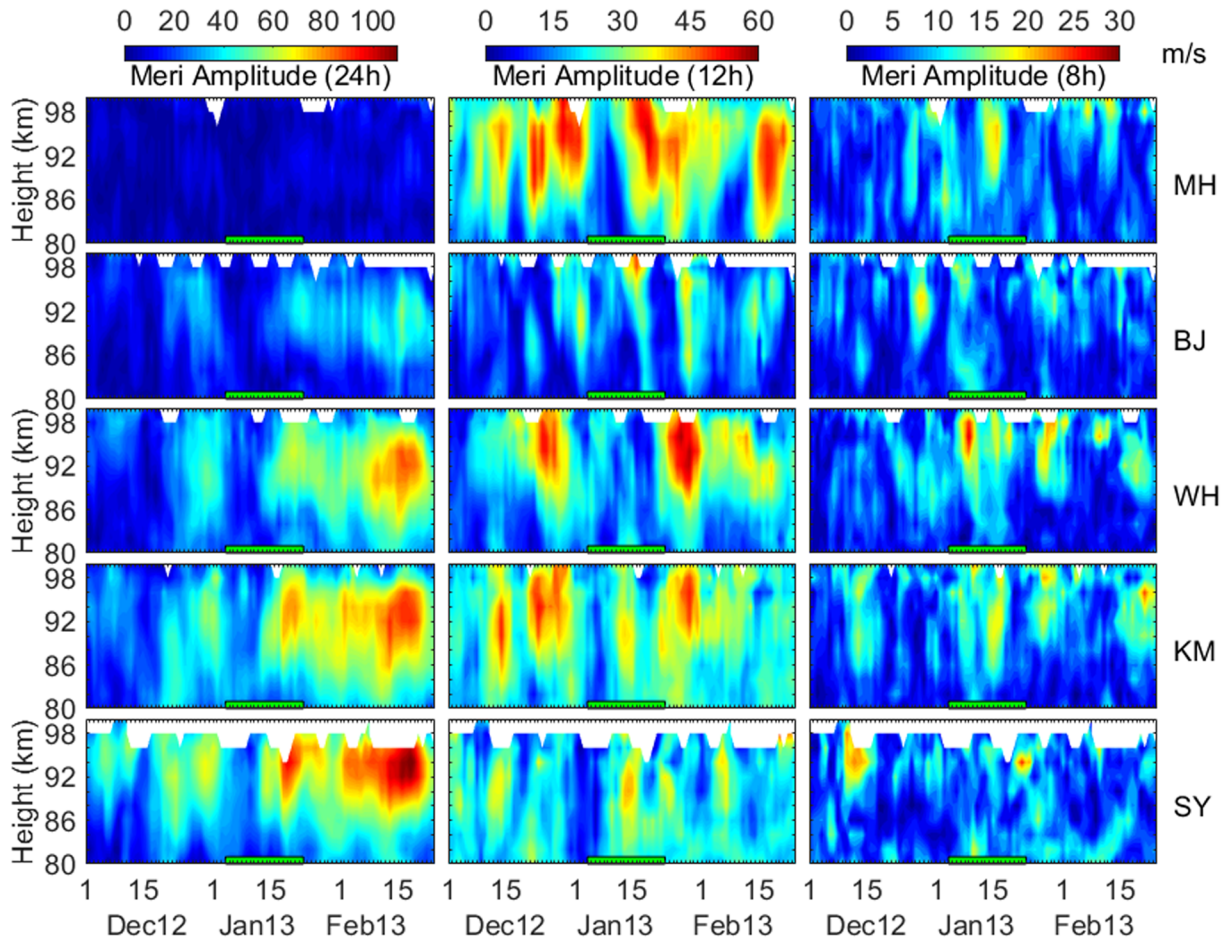

Figure 6. Similar with Figure 5 but for diurnal (left column), semidiurnal (middle column), and terdiurnal (right column) amplitudes in meridional winds.

SSW, the structure of daily variabilities was similar at Beijing, Wuhan, Kunming, and Sanya. However, during the 2013 SSW, the semidiurnal amplitude in the zonal wind decreased over Mohe, Beijing, and Wuhan. It decreased further after ~9 days and returned to its normal value at around 17 January over Mohe and Beijing. Whereas the semidiurnal amplitude in the zonal wind decreased before the SSW onset and increased during the SSW onset below 90 km at Kunming and below 94 km at Sanya. The variations of semidiurnal amplitude of the zonal wind before and after the 2013 SSW onset were small at all stations. Overall, there were significant fluctuations in the zonal semidiurnal tides over Wuhan, Kunming, and Sanya.

The semidiurnal amplitude of the meridional wind was comparable with that of the zonal wind over Mohe. From Wuhan to Sanya, the semidiurnal amplitude of the meridional wind decreased as the latitude decreased. A similar reduction was observed at all stations during the 2013 SSW. Specifically, the reduction of semidiurnal amplitude started from around 4 January at Mohe and Beijing, 3 January at Wuhan, 1 January at Kunming, and 29 December at Sanya. Soon after 7 January, the semidiurnal amplitude of meridional wind increased below 94 km at Kunming and Sanya. In other words, the influence of the SSW on the semidiurnal tide was largest at Mohe and gradually became weaken toward lower latitudes.

Comparing with the diurnal and semidiurnal tidal components, the terdiurnal tidal component demonstrated a strong inconsistency between zonal and meridional winds at all stations. As shown in Figures 5 and 6, the terdiurnal tidal amplitudes enhanced during the 2013 SSW, especially at middle latitudes. For instance, the increases in zonal terdiurnal amplitudes were observed during 14 to 20 January above 90 km at Mohe. On the other hand, the increases were observed during 2 to 6 January at all heights and 9 to 19 January below 86 km at Beijing. In the same vein, the increases were also observed during 9 to 17 January at all heights at Wuhan, 7 to 10 January at all heights at Kunming, and 12 to 17 January above

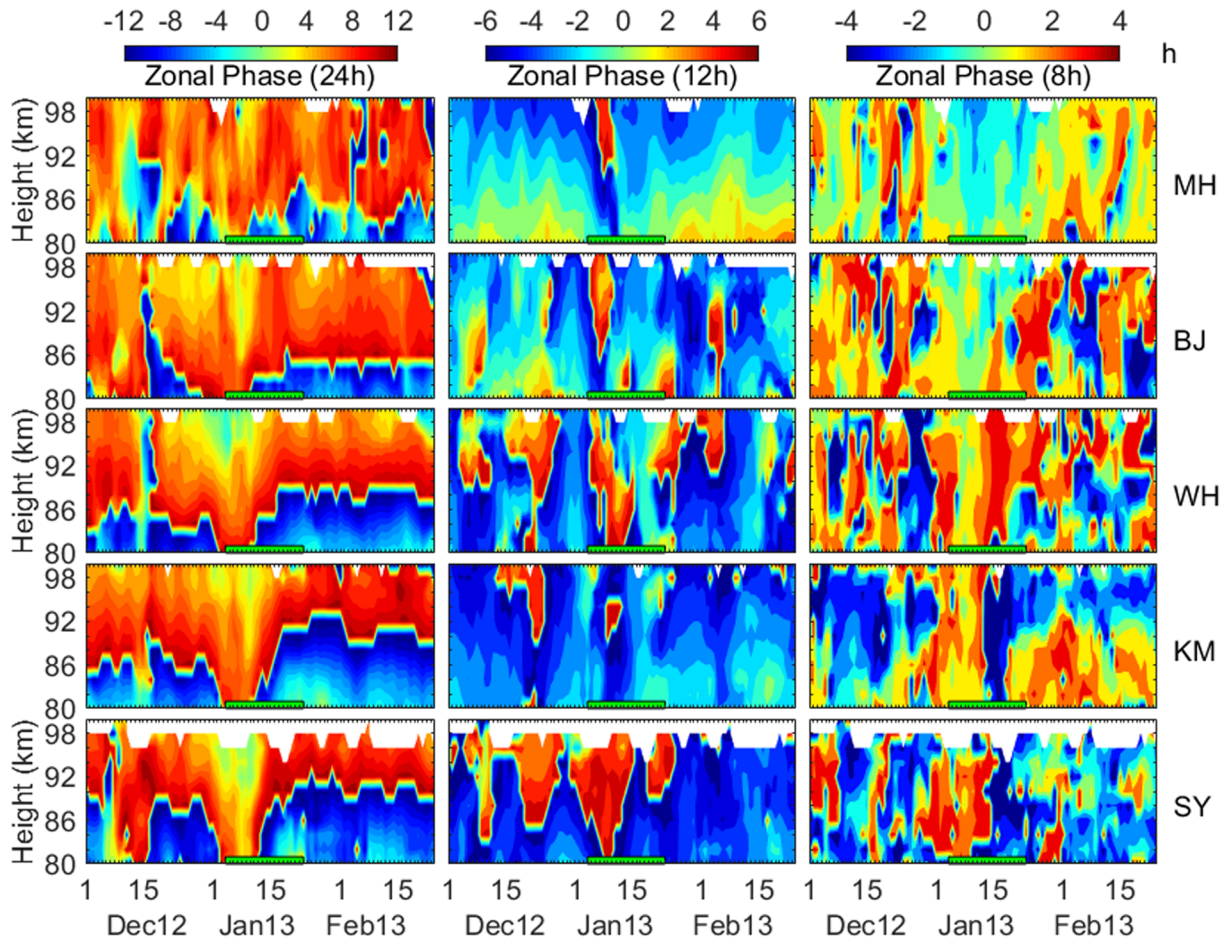

Figure 7. Variations of diurnal (left column), semidiurnal (middle column), and terdiurnal (right column) phases in zonal winds as a function of altitude and date during the 2013 SSW at Mohe, Beijing, Wuhan, Kunming, and Sanya.

90 km at Sanya. The increases of terdiurnal amplitude in meridional winds were seen from 13 to 17 January above 90 km at Mohe and at all heights at Beijing and Wuhan during 4–13 January and 6–19 January, respectively. Similar enhancement of the terdiurnal amplitude in meridional winds was also observed from 6 to 18 January above 84 km at Kunming and from 8 to 13 January below 84 km at Sanya. Thus, these increments were associated with the SSW effects considering the varying coverage of height and the magnitude of the amplitude variations. At each station, the terdiurnal amplitude of meridional wind was larger than that of zonal wind.

Figures 7 and 8 depict the tidal phases in zonal and meridional tides. It is clearly seen that the diurnal phase shifted to earlier time at all heights in the zonal and meridional winds. Note that the diurnal phase of meridional tide shifted toward a later time within the height range of 88–94 km at Mohe and of 96–100 km at Beijing. The shifting of the zonal tidal phase was related to the coupling processes from below to upper atmosphere (Fuller-Rowell et al., 2010). The variations in diurnal tidal phase in the zonal and meridional winds started from higher altitude and toward lower altitudes. For the semidiurnal tide, the phase of the zonal wind (Figure 7, middle column) recorded a large phase shifts in comparison with that of the meridional wind (Figure 8, middle column). The semidiurnal phase in the zonal wind moved earlier suddenly for few days and followed by a shift toward a later time. The lasting interval of this phase shifted toward a later time as the latitude decreased. For instance, the phase shifts in the zonal wind mainly occurred from 8 to 12 January above 90 km at Mohe and from 10 to 14 January within the height of 90–96 km at Kunming. Similarly, the semidiurnal phase of the meridional wind shifted toward a later time from 5 to 11 January and moved earlier after 11 January above 86 km at Mohe and Beijing. At other three stations (Wuhan,

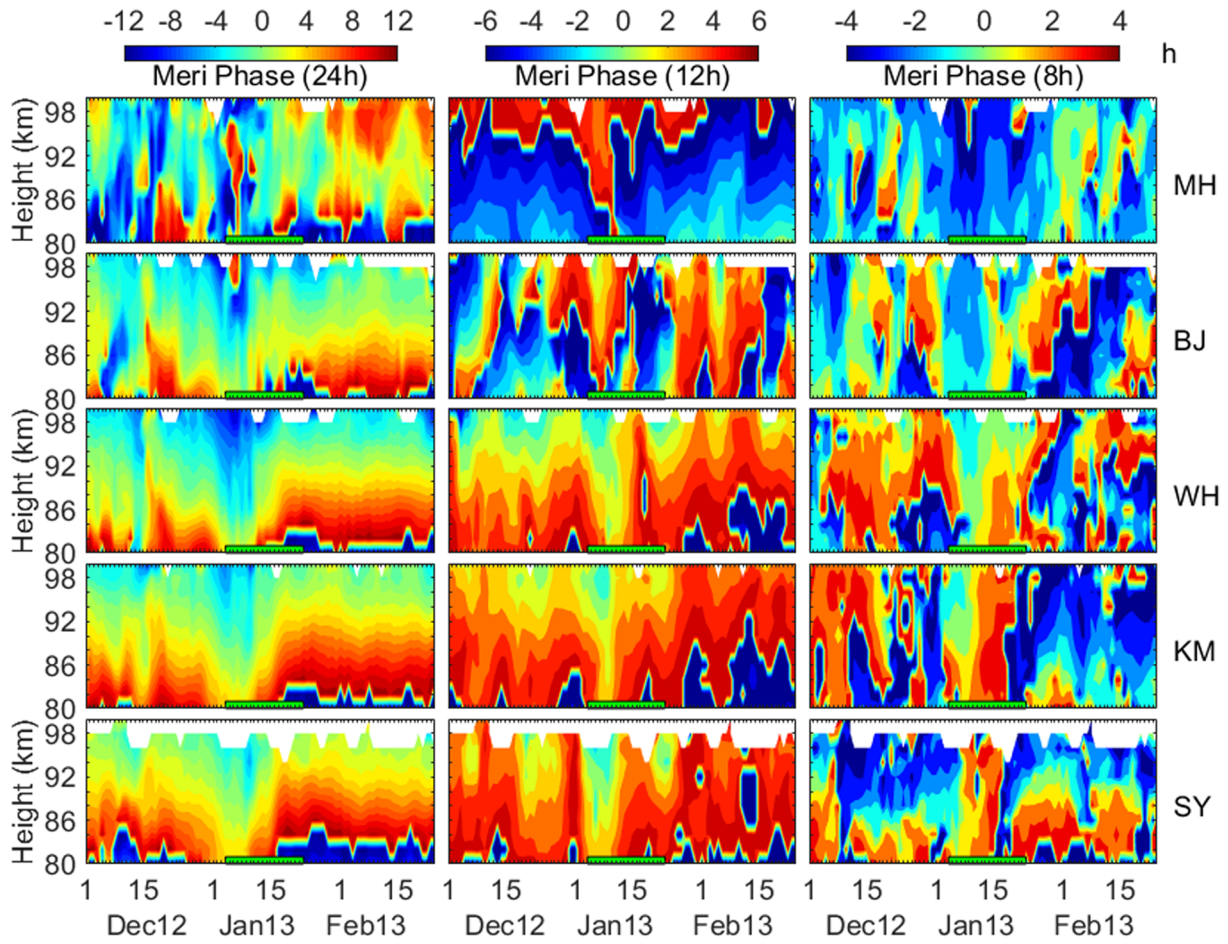

Figure 8. Similar with Figure 7 but for diurnal (left column), semidiurnal (middle column), and terdiurnal (right column) phases in meridional winds.

Kunming, and Sanya), the semidiurnal phase of the meridional wind shifted to earlier time from 7 to 11 January at all heights. Meanwhile, the terdiurnal phase also shifted to earlier time in zonal and meridional winds, especially at Mohe, Beijing, and Wuhan. The terdiurnal phase shifted toward a later time followed by shifting to earlier time recorded in the zonal and meridional winds at Kunming and Sanya.

Figures 9 and 10 show the tidal vertical wavelengths in zonal and meridional winds calculated from the corresponding tidal phases in Figures 7 and 8 (Jiang et al., 2009). It can be seen that the tidal wavelengths in neutral winds showed larger oscillations at lower latitudes (Wuhan, Kunming, and Sanya) than those at higher latitudes (Mohe and Beijing) in response to the SSW. As shown in Figure 9, the diurnal tidal wavelength of zonal wind increased prominently at Beijing, Kunming, and Sanya. Specifically, it reached as large as 120 km at Kunming when the diurnal amplitude had a decrease. Interestingly, the semidiurnal tidal wavelength in the zonal wind showed a large increase at all latitudes, even before the SSW. It had the peak value being as large as 85–90 km at Mohe and Beijing and a bit more than 110 km at Wuhan, Kunming, and Sanya. The terdiurnal tidal wavelength in the zonal wind also increased at Beijing, Wuhan, and Kunming. For the meridional wind (Figure 10), the semidiurnal and terdiurnal tidal wavelengths showed great increments in response to the SSW. For example, the maximum wavelength at Wuhan reached as large as 180 km for semidiurnal and 130 km for terdiurnal tide. Note that the diurnal tidal wavelength in the meridional wind displayed unexpected oscillations in the SSW onset at all stations. These results indicated that the wave-mean flow and wave-wave interactions affected not only the tidal amplitude and phase but also the tidal vertical structure.

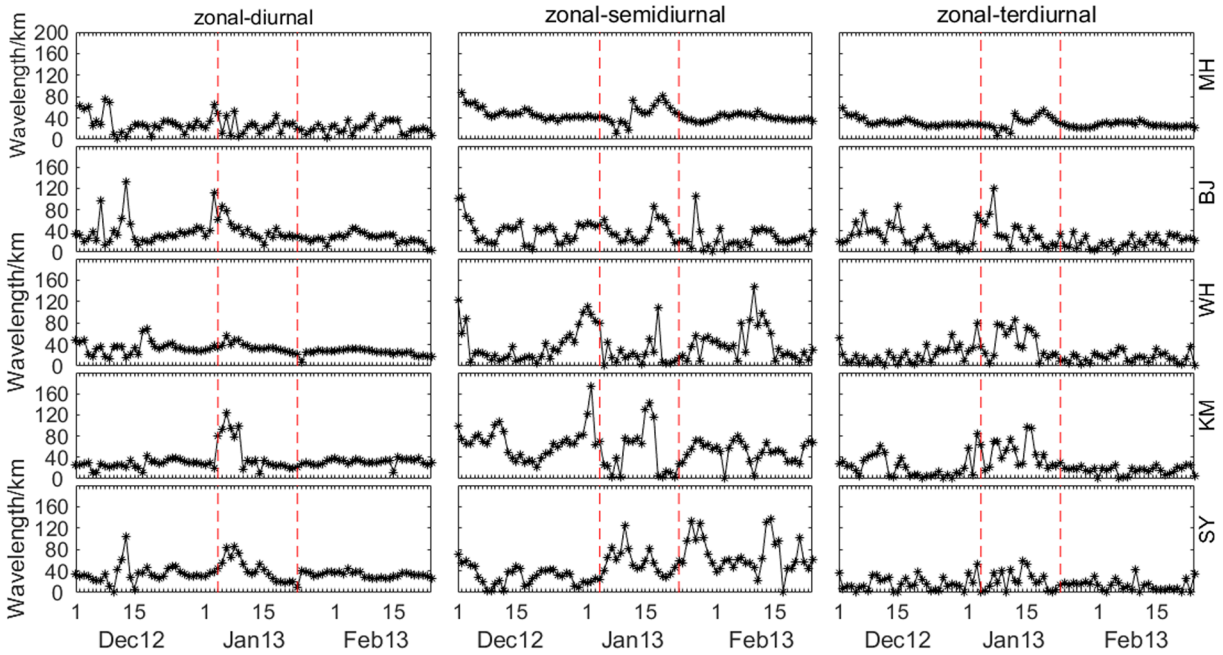

Figure 9. Variations of vertical wavelengths of diurnal (left column), semidiurnal (middle column), and terdiurnal (right column) tidal components in zonal winds.

4. Discussion

The results in Figures 4–6 showed that both the mean wind and tidal amplitudes displayed multiple peaks even during the non-SSW period. For instance, the semidiurnal amplitude at Mohe peaked on 4, 10, 15–16, and 23 December and the meridional tides above 86 km showed peaks on 9, 12–15, and 21–24 December, and 27 December to 2 January. These results revealed the possible interactions between tides and PWs.

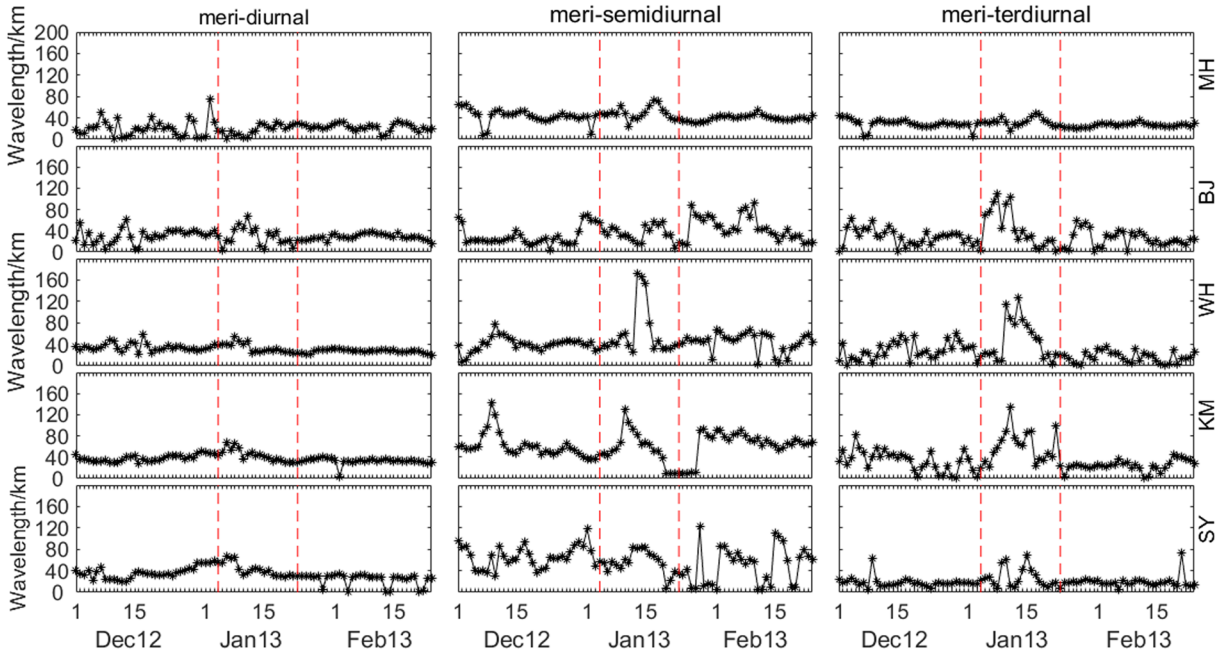

Figure 10. Variations of vertical wavelengths of diurnal (left column), semidiurnal (middle column), and terdiurnal (right column) tidal components in meridional winds.

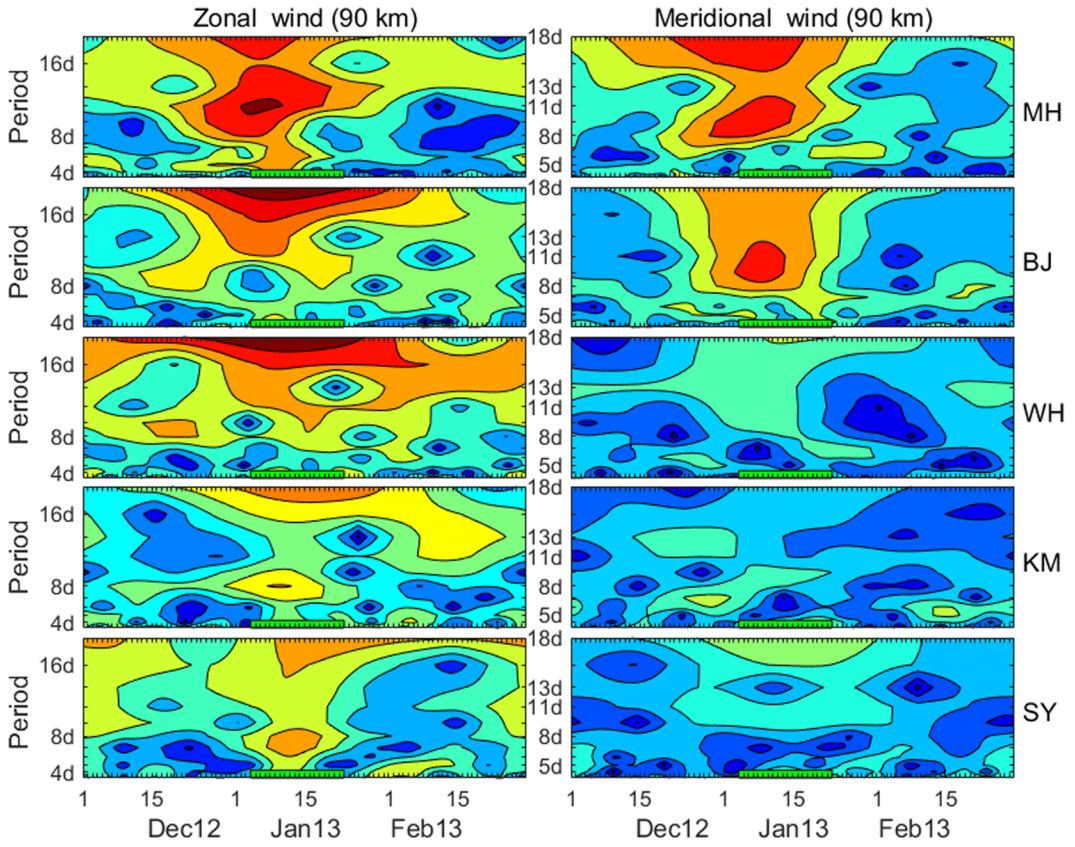

Figure 11. Wavelet spectra of zonal (left column) and meridional (right column) winds at 90 km at Mohe, Beijing, Wuhan, Kunming, and Sanya during the 2013 SSW.

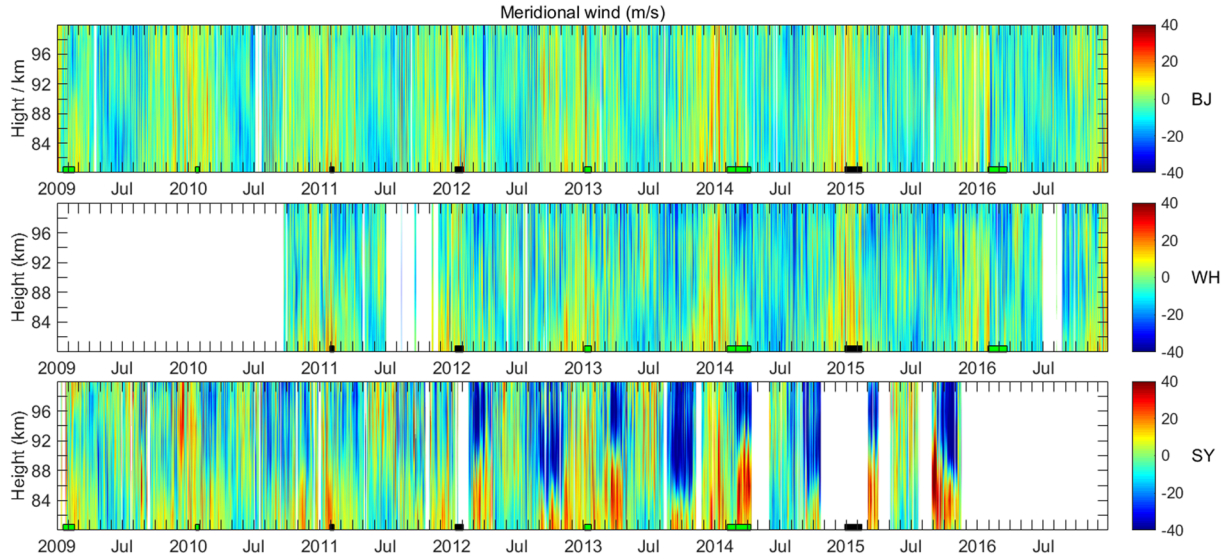

Figure 12. Meridional winds at Beijing, Wuhan, and Sanya stations during 2009–2016. The black bars represent minor SSW events, and the green bars denote major SSW events.

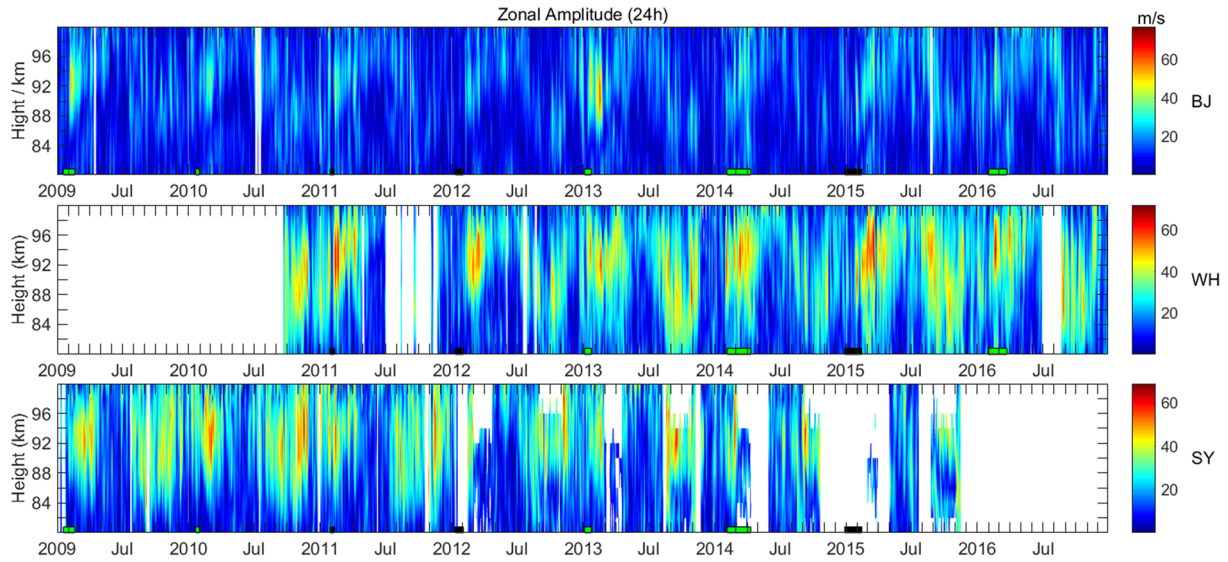

Figure 13. Variations of diurnal amplitudes of zonal winds at Beijing, Wuhan, and Sanya during 2009–2016.

Figure 11 shows the Morlet wavelet spectra of the hourly averaged zonal and meridional winds at 90 km during the 2013 SSW. It can be seen that at all stations the fluctuation amplitudes with periods of 8 to 11 and 16 to 18 days increased, while the diurnal and semidiurnal amplitudes decreased during the 2013 SSW. The terdiurnal amplitudes in both wind components increased below 90 km at Mohe. Consequently, the wave oscillations at the periods of about 16 and 11 days dominated during 1–18 January at Mohe. The diurnal and semidiurnal amplitudes of zonal and meridional winds at Beijing decreased, while the planetary oscillations with periods of 11 to 18 days in the zonal tide and 8 to 11 days in the meridional tide became strengthened. Additionally, the terdiurnal amplitude of zonal wind increased with largest increment of 7 m/s and the meridional wind increased with largest increment of 4 m/s below 86 km, as the period of PW increased. As shown in Figures 5, 6, and 11, the PW with the period of 6 to 18 days was weaker in the meridional wind and was stronger in the zonal wind around 1–18 January, when the diurnal and semidiurnal amplitudes decreased at Wuhan. The enhancement of terdiurnal amplitude could be related to the changes in planetary periods of 6 to 18 days. Different from the situation at Wuhan, the dominating periods of PWs at Kunming were 8 and 16 to 18 days in the zonal wind and only 8 days in the meridional wind. The decrease in diurnal amplitude of zonal wind and increase in PWs with the periods of 6 to 8 and 16 to 18 days may be responsible for the increase in the semidiurnal and terdiurnal amplitudes at Sanya. Additionally, the responses of terdiurnal amplitude to the 2013 SSW in the meridional wind at Sanya were mainly attributed to the changes in PWs, diurnal, and semidiurnal tides.

As shown in Figures 5 and 6, there was obvious latitudinal-dependent structure of the tidal waves during the 2013 SSW. The altitudinal range, where the semidiurnal amplitude decreased, became lower with latitude decreasing. In particular, the semidiurnal amplitude enhanced at lower latitudes (Kunming and Sanya) from 12 to 16 January. As shown in Figure 11, the periodic oscillations of quasi 8 and 11 days dominated the neutral wind at the middle latitudes (Mohe, Beijing, and Wuhan) and those with the period of quasi 6 to 8 days were prevailing at lower latitudes (Kunming and Sanya). The amplitude of PW increased as the tidal amplitude decreased. Hence, the difference in tidal amplitudes at middle and lower latitudes was caused by the interactions between PWs and tidal waves.

It should be noted that the amplitudes of diurnal and semidiurnal tides at Mohe were clearly different from those at other four stations. This feature is expected since the tidal components are dominated by the first two symmetric modes and the first two antisymmetric modes of Hough functions. These two modes suggested that the diurnal tidal wave energy mainly deposits within the latitudinal range of −49°N to 49°N, whereas most of the semidiurnal tidal wave energy was deposited at the middle and high latitudes. For

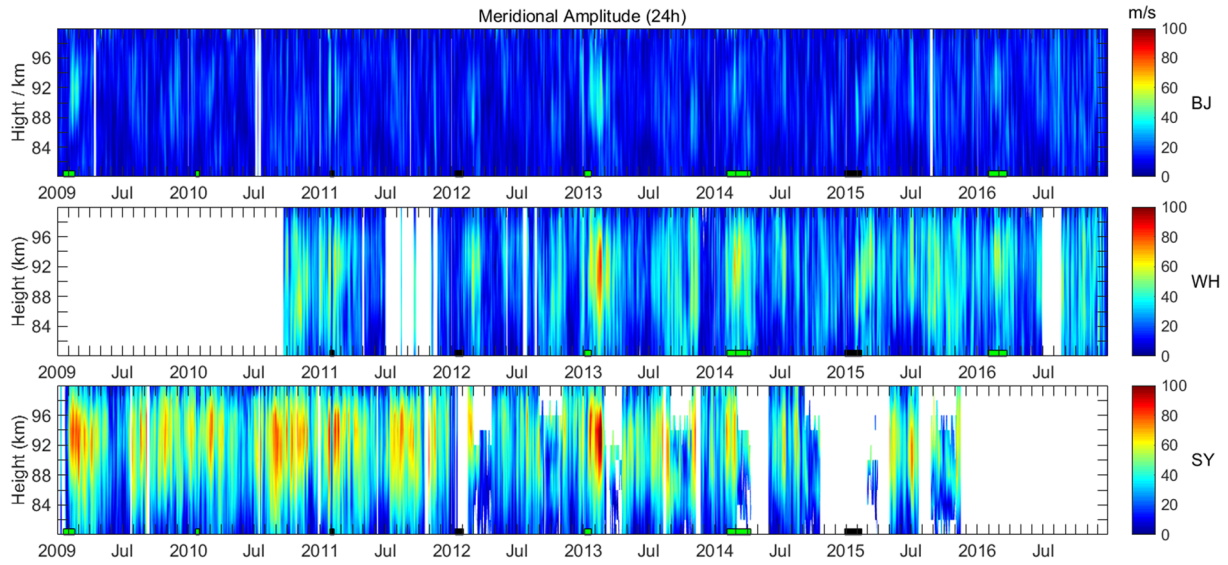

Figure 14. Variations of diurnal amplitudes of meridional winds at Beijing, Wuhan, and Sanya during 2009–2016.

the reason that Mohe (53.5°N) is located outside the range of −49°N to 49°N, the tidal amplitude at Mohe is different from those at other stations.

As shown in Figure 4, the westward wind prior to the SSW onset at low-middle latitudes (Kunming and Sanya) was generally consistent with the previous works carried out by using the observations at low-middle and high latitudes (Bhattacharya et al., 2004; Chen et al., 2012; Dowdy et al., 2007; Hoffmann et al., 2007; Jacobi et al., 2003; Sathishkumar et al., 2009; Xiao et al., 2014). Note that the northward wind got strengthened during the 2013 SSW, though the northward wind was always expected to be weaken and reversed to southward during the SSW events (Chen et al., 2012; Dowdy et al., 2007; Sathishkumar & Sridharan, 2009; Wang & Alexander, 2009). As seen in Figures 5 and 6, there were large increments in the diurnal amplitude from 13 January to the end of February. In order to identify whether these increments were related to the seasonal variation, the SSW effects, or other factors, we obtained the observations of neutral winds from the year 2009 to 2016 over Beijing, Wuhan, and Sanya. The meridional wind and diurnal amplitudes in zonal and meridional winds during these periods are shown in Figures 12–14. During this period, eight SSW events were occurred, including three minor events (labeled with black color) and five major events (labeled with green color). The information on these eight events is given in Table 2. In comparing these with the increment in the northward wind of Figure 12, we observed that the enhancement of northward wind during the 2013 SSW was a unique phenomenon among these eight events. Dunkerton and Butchart (1984) suggested that the enhancements of 16-day PWs may be caused by the increments in the northward winds. In addition, the mechanism causing variations in the tidal waves was partly induced by the temperature changes during the SSW and also by the forcing circulation from PWs (Sridharan, 2017). Consequently, the increment of the northward wind may induce the enhancement of quasi 16-day wave and then further influenced the nonlinear interactions of wave-wave and wave-mean flow.

Table 2
Information of SSWs During 2009–2016

Year	Starting date	Ending date	Classification
2009	16 Jan	19 Feb	Major
2010	20 Jan	10 Feb	Major
2011	28 Jan	9 Feb	Minor
2012	11 Jan	3 Feb	Minor
2013	4 Jan	23 Jan	Major
2014	4 Feb	11 Apr	Major
2014–2015	29 Dec	13 Feb	Minor
2016	29 Jan	22 Mar	Major

It is also noted from Figure 4 that the westward wind above the altitude of ~88 km had the short-periodic oscillations at the middle latitude. In addition, the semidiurnal amplitudes were subjected to a dramatic decrease followed by a great increase during the 2013 SSW, which was not consistence with the increment in semidiurnal amplitude previously reported (McCormack et al., 2017). These discrepancies call for further investigations by using observations and numerical simulations.

By comparing Figures 5, 6, 9, and 10, during the 2013 SSW, the decreased semidiurnal amplitude corresponded to an increase in semidiurnal tidal

wavelength, whereas the terdiurnal amplitude increased with the increase of terdiurnal tidal wavelength especially at Beijing, Wuhan, and Kunming. Therefore, the wave packet of semidiurnal tide may be dragged in one direction, and the wave packet of terdiurnal tide was spread out from inside to outside. These variations of wave packet, which are related to the SSW, are a worthy point in the future investigation.

Figures 13 and 14 display the diurnal tidal amplitude from 2009 to 2016 in zonal and meridional winds, respectively. The diurnal amplitude of zonal winds increased prominently after the 2013 SSW, especially at Beijing. Meanwhile, the diurnal amplitude in meridional winds after the 2013 SSW increased greatly at three stations. It is noted that the increased magnitude of zonal and meridional diurnal tides in 2013 was largest from 13 January to the end of February, though the increase of zonal and meridional diurnal tides occurs in every year. Consequently, the regular increase of diurnal tide with a small magnitude should be related to its seasonal variation, but the remarking amplitude of diurnal tides could be associated with the 2013 SSW. Nevertheless, more long-term wind observations and theoretical investigations are desirable to further assess this aspect.

5. Conclusions

Meteor radar observations from 1 December 2012 to 28 February 2013 within the latitudinal range of 18–53° N were utilized to study the responses of neutral winds and tides in the MLT to the 2013 SSW. It was found that, during the 2013 SSW, the westward reversal occurred as expected, but the northward wind suddenly increased in response to the onset of the SSW. Meanwhile, the amplitude of northward wind decreased with the decreasing latitude from Mohe to Kunming. The diurnal and semidiurnal amplitudes showed a decrease from around 5 to 13 January followed by an increase after 13 January. At the same time, the terdiurnal amplitude increased at all stations and was larger at Beijing, Wuhan, and Kunming than that at Sanya.

The diurnal and terdiurnal phases shifted to earlier time during the 2013 SSW. Futhermore, the semidiurnal phases also shifted to earlier time and followed by a shift toward a later time at higher height. The changes of tidal phases also reflected in the tidal wavelength. The semidiurnal wavelength in the zonal tide increased greatly at all stations, and the wavelength in terdiurnal tide showed an increase at Beijing, Wuhan, and Kunming stations. However, the diurnal wavelength of the meridional wind showed weak oscillations at all stations.

The tide-PW interactions could play an important role in modulating the behaviors of MLT region during the SSW. The changes in tidal waves and PW periods indicated that the nonlinear interactions between them were complex during the SSW event. Moreover, the 8-year observation of neutral winds and its tidal components revealed that the 2013 SSW was a unique event, in which there was a prominent increment in the northward wind after the SSW.

Acknowledgments
This work is supported by the B-type Strategic Priority Program of the Chinese Academy of Sciences (XDB41000000), and the National Science Foundation of China (41831070 and 41974181), the Fundamental Research Funds for the Central Universities, and the Open Research Project of Large Research Infrastructures of CAS—"Study on the interaction between low/mid-latitude atmosphere and ionosphere based on the Chinese Meridian Project". Luan X. was also supported by the National Natural Science Foundation of China (41874184 and 41674154). Li N. is supported by the National Science Foundation of China (41604129) and Taishan Scholar Program of Shandong Province, China. We acknowledge the use of data from the Chinese Meridian Project (https://data.meridianproject.ac.cn/). The Mohe, Beijing, Wuhan, and Sanya meteor radar data are provided by BNOSE, IGGCAS through the Data Center for Geophysics, National Earth System Science Data Sharing infrastructure (http://wdc.geophys.cn/). The authors are very thankful to NCEP/NCAR reanalysis team for providing access (https://www.esrl.noaa.gov/psd/data/gridded/tables/daily.html) to the stratospheric temperature and zonal mean zonal wind measurements used in this study.

References

Beard, A., Mitchell, N., Williams, P., & Kunitake, M. (1999). Non-linear interactions between tides and planetary waves resulting in periodic tidal variability. *Journal of Atmospheric and Solar-Terrestrial Physics*, *61*(5), 363–376. http://doi.org/10.1016/S1364-6826(99)00003-6

Bhattacharya, Y., Shepherd, G. G., & Brown, S. (2004). Variability of atmospheric winds and waves in the Arctic polar mesosphere during a stratospheric sudden warming. *Geophysical Research Letters*, *31*, L23101. http://doi.org/10.1029/2004GL020389

Bolaji, O. S., Oyeyemi, E. O., Owolabi, O. P., Yamazaki, Y., Rabiu, A. B., Okoh, D., et al. (2016). Solar quiet current response in the African sector due to a 2009 sudden stratospheric warming event. *Journal Geophysical Research: Space Physics*, *121*, 8055–8065. http://doi.org/10.1002/2016JA022857

Chandran, A., Collins, R. L., & Harvey, V. L. (2014). Stratosphere-mesosphere coupling during stratospheric sudden warming events. *Advances in Space Research*, *53*, 1265–1289. https://doi.org/10.1016/j.asr.2014.02.005

Chandran, A., Garcia, R. R., Collins, R. L., & Chang, L. C. (2013). Secondary planetary waves in the middle and upper atmospheric following the stratospheric sudden warming event of January 2012. *Geophysical Research Letters*, *40*(9), 1861–1867. https://doi.org/10.1002/grl.50373

Chen, X., Hu, X., & Xiao, C. (2012). Variability of MLT winds and waves over mid latitude during the 2000/2001 and 2009/2010 winter stratospheric sudden warming. *Annales de Geophysique*, *30*, 991–1001. http://doi.org/10.5194/angeo-30-991-2012

Coy, L., Eckemann, S. D., Hoppel, K. W., & Sassi, F. (2011). Mesospheric precursors to the major stratospheric sudden warming of 2009: Validation and dynamical attribution using a ground-to-edge-of-space data assimilation system. *Journal of Advances in Modeling Earth System*, *3*, M10002. https://doi.org/10.1029/2011MS000067

Dowdy, A. J., Vincent, R. A., Tsutsumi, M., Igarashi, K., Murayama, Y., Singer, W., et al. (2007). Polar mesosphere and lower thermosphere dynamics: 2. Response to sudden stratospheric warmings. *Journal Geophysical Research*, *112*, D17105. http://doi.org/10.1029/2006JD008127

Dunkerton, T., & Butchart, N. (1984). Propagation and selective transmission of internal gravity waves in a sudden warming. *Journal of the Atmospheric Sciences*, *41*(8), 1443–1460. http://doi.org/10.1175/1520-0469(1984)041<1443:pastoi>2.0.co;2

Fuller-Rowell, T., Wu, F., Akmaev, R., Fand, T., & Araujo-Pradere, E. (2010). A whole atmosphere model simulation of the impact of a sudden stratospheric warming on thermosphere dynamics and electrodynamics. *Journal of Geophysical Research*, *115*, A00G08. https://doi.org/10.1029/2010JA015524

He, M., Chau, J. L., Stober, G., Hall, C. M., Tsutsumi, M., & Hoffmann, P. (2017). Application of Manley-Rowe relation in analyzing nonlinear interactions between planetary waves and the solar semidiurnal tide during 2009 sudden stratospheric warming event. *Journal of Geophysical Research: Space Physics*, *122*, 10,783–10,795. http://doi.org/10.1002/2017JA024630

Hoffmann, P., Singer, W., Keuer, D., Hocking, W. K., Kunze, M., & Murayama, Y. (2007). Latitudinal and longitudinal variability of mesospheric winds and temperatures during stratospheric warming events. *Journal of Atmospheric and Solar-Terrestrial Physics*, *69*(17–18), 2355–2366. http://doi.org/10.1016/j.jastp.2007.06.010

Holdsworth, D. A., Reid, I. M., & Cervera, M. A. (2004). Buckland Park all-sky interferometric meteor radar. *Radio Science*, *39*, RS5009. http://doi.org/10.1029/2003RS003014

Jacobi, C., Kürschner, D., Muller, H. G., Pancheva, D., Mitchell, N. J., & Naujokat, B. (2003). Response of the mesopause region dynamics to the February 2001 stratospheric warming. *Journal of Atmospheric and Solar-Terrestrial Physics*, *65*(7), 843–855. http://doi.org/10.1016/S1364-6826(03)00086-5

Jiang, G., Xu, J., & Franke, S. J. (2009). The 8-h tide in the mesosphere and lower thermosphere over Maui (20.75°N, 156.43°W). *Annales Geophysicae*, *27*(5), 1989–1999. https://doi.org/10.5194/angeo-27-1989-2009

Kalnay, E., Kanamitsu, M., Kistler, R., Collins, W., Deaven, D., Gandn, L., et al. (1996). The NCEP/NCAR 40-year reanalysis project. *Bulletin of American Meteorological Society*, *77*(3), 437–471. https://doi.org/10.1175/1520-0477(1996)077<0437:TNYRP>2.0.CO;2

Koushik, N., Kumar, K. K., Ramkumar, G., & Subrahmanyam, K. V. (2018). Response of equatorial and low latitude mesosphere lower thermospheric dynamics to the northern hemispheric sudden stratospheric warming events. *Journal of Atmospheric and Solar-Terrestrial Physics*, *169*(2018), 66–77. https://doi.org/10.1016/j.jastp.2018.01.021

Labitzke, K., & Naujokar, B. (2000). The lower Arctic stratosphere in winter since 1952. *SPARC Newsletter*, *15*, 11–14.

Lima, L. M., Alves, E. O., Batista, P. P., Clemesha, B. R., Medeiros, A. F., & Buriti, R. A. (2012). Sudden stratospheric warming effects on the mesospheric tides and 2-day wave dynamics 7°S. *Journal of Atmospheric and Solar-Terrestrial Physics*, *78-79*, 99–107. http://doi.org/10.1016/j.jastp.2011.02.013

Lin, C. H., Lin, J. T., Chang, L. C., Liu, J. Y., Chen, C. H., Chen, W. H., et al. (2012). Observations of global ionospheric responses to the 2009 stratospheric sudden warming event by FORMOSAT-3/COSMIC. *Journal Geophysical Research*, *117*, A06323. http://doi.org/10.1029/2011JA017230

Liu, L., Liu, H., Le, H., Chen, Y., Sun, Y.-Y., Ning, B., et al. (2017). Mesospheric temperatures estimated from the meteor radar observations at Mohe, China. *Journal of Geophysical Research: Space Physics*, *122*, 2249–2259. http://doi.org/10.1002/2016JA023776

Ma, Z., Gong, Y., Zhang, S. D., Zhou, Q. H., Huang, C. M., Huang, K. M., et al. (2017). Responses of quasi 2 day waves in the MLT region to the 2013 SSW revealed by a meteor radar chain. *Geophysical Research Letters*, *44*, 9142–9150. http://doi.org/10.1002/2017GL074597

Martineau, P., & Son, S. W. (2015). Toward a general solution of the three-wave partial differential equations. *Studies in Applied Mathematics*, *137*(1), 70–92. https://doi.org/10.1111/sapm.12133

Matsuno, T. (1971). A dynamical model of the stratospheric sudden warming. *Journal of Atmospheric Science*, *28*(8), 1479–1494. http://doi.org/10.1175/1520-0469(1971)028<1479:adomts>2.0.c0:2

Matthias, V., Hoffmann, P., Rapp, M., & Baumgarten, G. (2012). Composite analysis of the temporal development of waves in the polar MLT region during stratospheric warmings. *Journal of Atmospehric and Solar-Terrestrial Physics*, *90-91*, 86–96. https://doi.org/10.1016/j.jastp.2012.04.004

McCormack, J., Hoppel, K., Kuhl, D., de Wit, R., Stober, G., Espy, P., et al. (2017). Comparison of mesospheric winds from a high-altitude meteorological analysis system and meteor radar observations during the boreal winters of 2009-2010 and 2012-2013. *Journal of Atmospheric and Solar-Terrestrial Physics*, *154*, 132–166. http://doi.org/10.1016/j.jastp.2016.12.007

Niciejewski, R., Wu, Q., Skinner, W., Gell, D., Cooper, M., Marshall, A., et al. (2006). TIMED Doppler interferometer on the thermosphere ionosphere mesosphere energetics and dynamic satellite: Data product overview. *Journal of Geophysical Research*, *111*, A11S90. http://doi.org/10.1029/2005JA011513

Owolabi, C., Lei, J., Bolaji, O. S., Jimoh, O., Ruan, H., Li, N., et al. (2019). Investigation on the variability of the geomagnetic daily current during sudden stratospheric warmings. *Journal of Geophysical Research: Space Physics*, *124*, 6156–6172. http://doi.org/10.1029/2019JA026667

Pancheva, D., Mukhtarov, P., Mitchell, N. J., Andonov, B., Merzlyakov, E., Singer, W., et al. (2008). Latitudinal wave coupling of the stratosphere and mesosphere during the major stratospheric warming in 2003/2004. *Annales Geophysicae*, *26*(3), 467–483. http://doi.org/10.5194/angeo-26-467-2008

Pedatella, N. M., & Forbes, J. M. (2010). Evidence for stratosphere sudden warming-ionosphere coupling due to vertically propagating tides. *Geophysical Research Letters*, *37*, L11104. http://doi.org/10.1029/2010GL043560

Pedatella, N. M., & Liu, H.-L. (2013). The influence of atmospheric tide and planetary wave variability during sudden stratosphere warmings on the low latitude ionosphere. *Journal of Geophysical Research: Space Physics*, *118*, 5333–5347. http://doi.org/10.1002/jgra.50492

Reed, R. (1963). On the cause of the stratospheric sudden warming phenomenon. *Meteorology Abhand*, *36*, 315–334.

Sassi, F., Liu, H. L., Ma, J., & Garcia, R. R. (2013). The lower thermosphere during the northern hemisphere winter of 2009: A modeling study using high-altitude data assimilation products in WACCM-X. *Journal of Geophysical Research: Space Physics*, *118*, 8954–8969. http://doi.org/10.1002/jgrd.50632

Sathishkumar, S., & Sridharan, S. (2009). Planetary and gravity waves in the mesosphere and lower thermosphere region over Tirunelveli (8.71°N, 77.81°E) during stratospheric warming events. *Geophysical Research Letters*, *36*, L07806. http://doi.org/10.1029/2008GL037081

Sathishkumar, S., & Sridharan, S. (2013). Lunar and solar tidal variabilities in mesospheric winds and EEJ strength over Tirunelveli (8.7°N, 77.8°E) during the 2009 major stratospheric warming. *Journal of Geophysical Research: Space Physics*, *118*, 533–541. http://doi.org/10.1029/2012JA018236

Sathishkumar, S., Sridharan, S., & Jacobi, C. (2009). Dynamical response of low-latitude middle atmosphere to major sudden stratospheric warming events. *Journal of Atmospheric and Solar-Terrestrial Physics*, *71*, 857–865. http://doi.org/10.1016/j.jastp.2009.04.002

Shepherd, M. C., Wu, D. L., Fedulina, L. N., Gurubaran, S., Russell, J. M., Mlynczak, M. G., & Shepherd, G. G. (2007). Stratospheric warming effects on the tropical mesospheric temperature field. *Journal of Atmospheric and Solar-Terrestrial Physics*, *69*, 2309–2337. http://doi.org/10.1016/j.jastp.2007.04.009

Siddiqui, T. A., Luhr, H., Stolle, C., & Park, J. (2015). Relation between stratospheric sudden warming and the lunar effect on the equatorial electrojet based on Huancayo recordings. *Annales Geophysicae*, *33*(2), 235–243. http://doi.org/10.5194/angeo-33-235-2015

Siskind, D. E., Eckermann, S. D., McCormack, J. P., Coy, L., Hoppel, K. W., & Baker, N. L. (2010). Case studies of the mesospheric response to recent minor, major, and extended stratospheric warmings. *Journal of Geophysical Research*, *115*, D00N03. https://doi.org/10.1029/2010JD014114

Sridharan, S. (2017). Variabilities of low latitude migrating and nonmigrating tides in GPS-TEC and TIMED-SABER temperature during the sudden stratospheric warming event of 2013. *Journal of Geophysical Research: Space Physics*, *122*, 10,748–10,761. https://doi.org/10.1002/2017JA024283

Wang, L., & Alexander, M. J. (2009). Gravity wave activity during stratospheric sudden warmings in the 2007-2008 Northern Hemisphere winter. *Journal of Geophysical Research*, *114*, D18108. http://doi.org/10.1029/2009JD011867

Wit, R. J., Hibbins, R. E., Espy, P. J., & Hennum, E. A. (2015). Coupling in the middle atmosphere related to the 2013 major sudden stratospheric warming. *Annales de Geophysique*, *33*, 309–319. https://doi.org/10.5194/angeo-33-309-2015

Xiao, C., Hu, X., & Xu, Q. (2014). Response of mesosphere and lower thermosphere wind over mid-latitude to the 2013 major sudden stratospheric warming event. In *31th URSI General Assembly and Scientific Symposium, URSI GASS*. Beijing, China. August 16–23, 2014.

Xiong, J., Wan, W., Ding, F., Liu, L., Ning, B., & Niu, X. (2013). Coupling between mesosphere and ionosphere over Beijing through semidiurnal tides during the 2009 sudden stratospheric warming. *Journal of Geophysical Research: Space Physics*, *118*, 2511–2521. http://doi.org/10.1002/jgra.50280

Yamashita, C., Liu, H. L., & Chu, X. (2010). Responses of mesosphere and lower thermosphere temperatures to gravity wave forcing during stratospheric sudden warming. *Geophysical Research Letters*, *37*, L09803. https://doi.org/10.1029/2009GL042351

Yamazaki, Y., Richmond, A. D., & Yumoto, K. (2012). Stratospheric warmings and the geomagnetic lunar tide: 1958–2007. *Journal Geophysical Research*, *117*, A04301. http://doi.org/10.1029/2012JA017514

Yu, Y., Wan, W., Ning, B., Liu, L., Wang, Z., Hu, L., & Ren, Z. (2013). Tidal wind mapping from observations of a meteor radar chain in December 2011. *Journal of Geophysical Research: Space Physics*, *118*, 2321–2332. http://doi.org/10.1029/2012JA017976

Yu, Y., Wan, W., Ren, Z., Xiong, B., Zhang, Y., Hu, L., et al. (2015). Seasonal variations of MLT tides revealed by a meteor radar chain based on Hough mode decomposition. *Journal of Geophysical Research: Space Physics*, *120*, 7030–7048. http://doi.org/10.1002/2015JA021276

Yuan, T., Thurairajah, B., She, C., Chandran, A., Collins, R. L., & Krueger, D. A. (2012). Wind and temperature response of midlatitude mesopause region to the 2009 sudden stratospheric warming. *Journal of Geophysical Research*, *117*, D09114. http://doi.org/10.1029/2011JD017142